الجمهورية الجزائرية الديمقراطية الشعبية

Populaire et Démocratique Algérienne République

وزارة التعليم العالى والبحث العلمي

Ministère de l'Enseignement Supérieur et de la Recherche Scientifique

جامع ــــة سعد دحلب البليدة (1) DAHLEB- 1

Université SAAD Blida



Faculty of Science and Technology

Department of Electronics

Master's Thesis

In partial fulfillment of the requirement for the master's degree of ST

Field: Electrical engineering

Option: Microelectronic

Topic

Optimization and finalization of a semiconductor gas sensor for carbon monoxide detection

Presented by: Thesis Number presented on June

GUIRAA Abdelhamid Micro4 17th, 2025

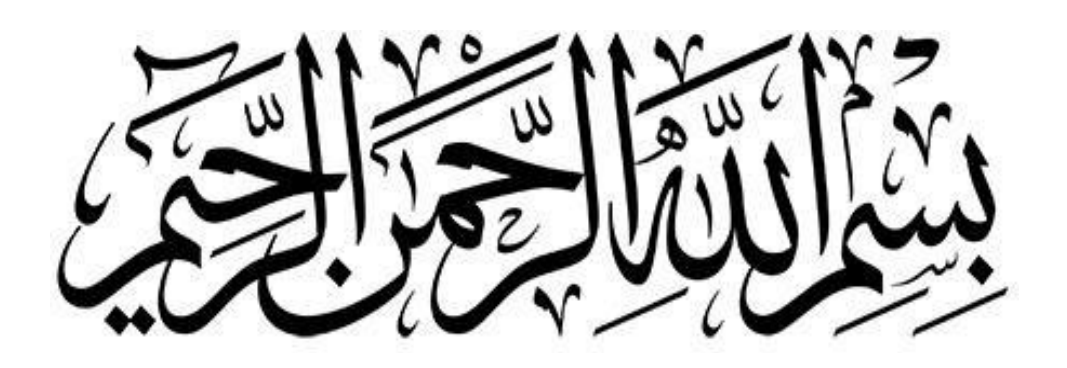
KESSOUM Ayoub

Submitted to the jury Quality

Mr Nacer Jury president

Mr Aliane Ecaminator

Mr Bounemri Supervisor



Acknowledgements

We would like to express our deepest gratitude to all those who contributed to the success of this final year project.

First and foremost, we would like to sincerely thank our supervisor, **Mr.Bounemri**, for his invaluable guidance, support, and encouragement throughout this project. His expertise and constructive feedback have been instrumental in shaping this work.

We also extend our heartfelt thanks to the president of the jury, **Mr. Nacer**, for his time, insightful comments, and valuable evaluation of my work.

Our sincere appreciation also goes to the examiner, **Mr. Aliane**, for his careful review, observations, and recommendations that greatly enriched the quality of this research.

Finally, we are grateful to everyone who, directly or indirectly, supported us throughout this academic journey.

Dedication

This work is dedicated to the journey, the challenges, and the determination that brought me here.

To myself — for the perseverance, the sleepless nights, and the constant efforts that made this achievement possible.

To my beloved family — for their unconditional love, encouragement, and endless support throughout every step of this journey.

To my dear friends — for their companionship, motivation, and belief in me, even during the toughest times.

Thank you all for being part of this accomplishment.



Abdelhamid

Dedication

I dedicate this work to the ones who have been by my side from the very beginning.

To myself — for the determination, resilience, and continuous efforts that led to this accomplishment.

To my dear parents, **Salim** and **Khalida** — thank you for your unconditional love, sacrifices, and constant encouragement. Your support has been my greatest strength.

To my sisters, **Assia** and **Fatima Zohra**— for always believing in me and cheering me on.

To my brother **Mohamed Lyes** — for his kindness, patience, and motivation during the challenging times.

This achievement is not mine alone; it belongs to all of you.



Ayoub

List of Abbreviations

CO: Carbon monoxide

A: Cross-sectional area (m²)

a: Intercept of line in logarithmic space

a, b: Coefficients of linear relation for n(T)

A, B: Constants in empirical relation

Au: Gold (electrode material)

b: Slope of line in logarithmic space

C°: Degrees Celsius

CCO: Gas concentration (ppm)

CO₂: Carbon dioxide

COV: Volatile organic compounds

e⁻: Electron

e: Thickness (m)

Ea: Activation energy (in eV)

eV: Electronvolt (unit of energy)

kB: Boltzmann constant $(8.617 \times 10^{-5} \text{ eV/K})$

L: Layer length (m)

Ln: Natural logarithm (logarithm base e)

MOX: Metal oxide semiconductors

N: Empirical coefficient/exponent (depends on temperature)

n(T): Exponent depending on temperature

NO₂: Nitrogen dioxide

 $\mathbf{O_{2}}^{-}, \mathbf{O}^{-}, \mathbf{O}^{2-}$: Adsorbed oxygen ionic species

O₃: Ozone

Ppm: Parts per million (concentration unit)

Pt: Platinum (heating material)

R: Electrical resistance of the sensor (Ω)

 $\mathbf{R}(\mathbf{C})$: Sensor resistance at concentration $\mathbf{C}(\Omega)$

R_air: Resistance in pure air (R₀)

R_gaz: Resistance in presence of CO

Ro: Reference resistance (in air or extrapolated/normalized)

R₀(T): Base resistance depending on temperature

R²: Coefficient of determination (fit quality)

R∞: Constant in Arrhenius law

S: Sensor sensitivity

Si: Silicon (substrate)

SiO₂: Silicon dioxide (insulator)

SSres: Sum of squared residuals

SStot: Total sum of squares

T: Absolute temperature (K) or temperature ($^{\circ}$ C) depending on context

W: Width (m)

x: ln(C), natural logarithm of CO concentration

y: ln(R), natural logarithm of resistance

ZnO: Zinc oxide

α: Concentration-related coefficient (m³/mol)

σ: Electrical conductivity (S/m)

 σ_0 : Pre-exponential conductivity constant

Figures list

Figure I.1. Overview of ZnO morphology	3
Figure I.2. Behavior of the exponent n of the power law in the presence of CO	4
Figure I.3. Multi-layer structure of a MOX sensor	5
Figure I.4. Variation in ZnO resistance as a function of CO concentration.	7
Figure II.1. Variation in ZnO resistance as a function of CO concentration.	9
Figure II.2. Linear regression ($T=200 \text{ oC}$) with $R2 = 0.933$	16
Figure II.3. ln(R) vs ln(C) fits for each temperature	17
Figure II.4. Variation of R as a function of T-dependent n and R0	19
Figure III.1. CO Sensor Sensitivity vs. CO Concentration	22
Figure III.2. Resistance vs. CO Concentration at Different Temperatures (T=100 Co)	23
Figure III.3. Resistance vs. CO Concentration at Different Temperatures (T=200 Co)	23
Figure III.4. Resistance vs. CO Concentration at Different Temperatures (T=300 Co)	24
Figure III.5. Resistance vs. CO Concentration at all Temperatures (global comparison)	25
Figure III.6. Experimental vs. Modeled Resistance of CO Gas Sensor at Varying	
Concentrations (T=100 Co)	27
Figure III.7. Experimental vs. Modeled Resistance of CO Gas Sensor at Varying	
Concentrations (T=200 Co)	28
Figure III.8. Experimental vs. Modeled Resistance of CO Gas Sensor at Varying	
Concentrations (T=3.00 Co)	29
Figure III.9. Experimental vs. Modeled Resistance of CO Gas Sensor at Varying	
Concentrations and all temperatures	30
	32
8 · · · · · · · · · · · · · · · · · · ·	33
	35
Figure III.13. Comparison of Experimental and Modeled Sensor Resistance at (T=200 Co)	
Figure III.14. Comparison of Experimental and Modeled Sensor Resistance at (T=300 Co)	36
Figure III.15. Comparison of Experimental and Modeled Sensor Resistance at at Varying	
Temperatures	37

Table list

Table I.1. 2D structure dimensions	6
Table II.1. (C.R) pairs	11
Table II.2. R vs CO concentration	12
Table II.3. Calculating logarithms	12
Table II.4. n as a function of temperature	13
Table II.5. Interpretation of R2	15
Table II.6. R0 as a function of temperature	18
Table II.7. the relation between T (°C), R0 measured and R0 estimated	19

Table of Contents

ACKNOWLEDGEMENTS

DEDICATION

LIST OF ABBREVIATIONS

FIGURES LIST

TABLE LIST

ABSTRACT

INTRODUCTION	. 1
CHAPTER I: STATE OF THE ART	.3
I .1. General introduction to gas sensors	. 3
I .2. Properties of ZnO for CO detection	.3
I .3. Empirical response modeling	.4
I .4. Numerical and experimental approaches	.5
I .5. Conclusion	.8
CHAPTER II: NECESSARY THEORIES	.9
II.1. Adsorption and surface chemical reaction	.9
II.2. Approximation of the law generating the variation of the resistance of ZnO as a function of the concentration of the gas CO	
II.3.Linear regression on data in logarithmic space	
II.4.Arrhenius law applied to R0	18
II.5.Sensor sensitivity	20
CHAPTER III: SIMULATION AND ANALYSIS OF RESULTS	21
III.1. Introduction	21
III.2. Methodology	21

III.3. Results	21
III.3.1. Sensor sensitivity trace	21
III.3.2. Comparison Between Experimental and Modeled Sensor Response to CO	
III.3.2.1 Conclusion	
III.3.3. Comparative Analysis of Experimental and Modeled CO Gas Sensor Responses	27
III.3.3.1 Conclusion	31
III.4. Coefficient n: nature and choice	31
III.4.1. RMSE (Root Mean Square Error): Role	32
III.4.1.1. Definition	32
III.4.1.2. Interpretation	32
III.4.2. Model Optimization	33
III.4.2.1_Conclusion	34
III.5. Experimental and Modeled Sensor Resistance	34
III.5.1 Conclusion	37
GENERAL CONCLUSION	40
BIBLIOGRAPHIC REFERENCES	40

الملخص

يعرض هذا البحث نموذجًا رياضيًا لمقاومة ZnO كدالة في تركيز غاز أول أكسيد الكربون وفق قانون القوة العكسية (R=R0(T)·C^{-n(T)} وذلك عند ثلاث درجات حرارة (100، 200، 300 درجة مئوية). تم استخراج المعاملين R0 و nمن البيانات التجريبية، و هما يعتمدان على درجة الحرارة. أظهرت النتائج تطابقًا جيدًا مع القيم المقاسة، مما يعزز دقة التنبؤ بأداء الحساس.

الكلمات المفتاحية :حساس غاز ، ZnO ، أول أكسيد الكربون، درجة الحرارة، النمذجة، قانون القوة العكسية

Résumé

Ce travail présente une modélisation de la résistance du ZnO en fonction de la concentration de CO, selon une loi de puissance inverse $R=R0(T)\cdot C^{-n(T)}$, à trois températures : 100, 200 et 300°C. Les paramètres R0 et n, extraits des données expérimentales, sont dépendants de la température. Les résultats obtenus permettent une bonne prévision de la réponse du capteur et une meilleure compréhension de son comportement.

Mots clés : capteur de gaz, ZnO, CO, température, modélisation, loi de puissance inverse

Abstract

This work presents a model of ZnO resistance as a function of CO concentration using an inverse power law $R=R0(T)\cdot C^{-n(T)}$, at three temperatures: $100^{\circ}C$, $200^{\circ}C$, and $300^{\circ}C$. The parameters R0 and n, derived from experimental data, are temperature-dependent. The results demonstrate good agreement with observed values and enable improved prediction and analysis of sensor behavior.

Keywords: gas sensor, ZnO, CO, temperature, modeling, inverse power law



Introduction

The monitoring of toxic gases in the environment and enclosed spaces has become a fundamental issue, both for public health and industrial safety. One of the most dangerous gases is carbon monoxide (CO), a colorless, odorless and highly toxic compound produced mainly by the incomplete combustion of organic matter. Because of its insidious nature, rapid and reliable detection of this gas is essential.

In this context, there is growing interest in sensors based on semiconducting metal oxides (MOX), in particular zinc oxide (ZnO). ZnO, as an n-type semiconductor, has a wide band gap (~3.3 eV), high electron mobility and remarkable sensitivity to various gases, including CO. At high temperatures, ZnO interacts with the chemical species present in air, resulting in a measurable change in its electrical resistance. This property is exploited in the manufacture of resistive gas sensors.

Previous work has shown that the resistance of ZnO varies empirically with the concentration of the target gas according to the law:

$$R=R0(T)\cdot C^{-n(T)}$$

Where R is the measured resistance, C the ppm concentration of the gas, R0 a temperature-dependent constant, and n an empirical coefficient that is also a function of temperature. For example, the doctoral thesis by M. Abbas B. (University of Constantine, 2017) [1] highlighted the impact of temperature on the sensitivity of ZnO to CO in a controlled environment. Other authors such as Yamazoe and Shimanoe (2009) have detailed the physico-chemical mechanisms of CO detection on metal oxide thin films, confirming that heating temperature plays a crucial role in the adsorption/reaction of gas molecules on the sensor surface [2][3].

More recently, several simulation studies have aimed to numerically and analytically model the electrical response of ZnO in different sensing contexts. For example, Wang et al (2020) proposed a sensor model based on the conductivity variation induced by the reaction of CO with adsorbed ionic species, while multiphysics finite element simulation coupled heat transfer, gas diffusion and electrical behavior in the sensor structure [4].

Introduction

This report aims to deepen our understanding of the resistive behavior of ZnO by proposing a mathematical model incorporating temperature dependence, and to validate this model with numerical simulation results. It is based both on established theoretical foundations and on a customized analysis based on empirical laws and physical parameters of the material. The report is structured as follows:

- Chapter I State of the art: presents an overview of research into ZnO-based sensors and the empirical or physical models used for CO detection.
- Chapter II Necessary theories: develops the scientific bases essential for understanding sensor operation, including surface reactions, Arrhenius law and sensitivity formulation.
- Chapter III Simulation and analysis of results: describes the simulation approach, the parameters chosen, the results obtained and their interpretation.
- **General conclusion:** summarizes the main contributions of the work and suggests ways of improving or extending the study.

I.1. General introduction to gas sensors

Gas sensors based on semiconductor oxides (MOX) represent a widely used technology for detecting pollutant gases such as carbon monoxide (CO), nitrogen dioxide (NO₂), ozone (O₃), or volatile organic compounds (VOCs). Among the most studied materials is zinc oxide (ZnO), which offers an interesting compromise between sensitivity, manufacturing cost, and chemical stability. MOX sensors generally operate on the principle of varying the conductivity of the material in the presence of the target gas. This principle is easy to exploit in the manufacture of compact, integrable sensors.

I.2. Properties of ZnO for CO detection

ZnO is an n-type semiconductor, crystallized in a hexagonal wurtzite structure, with a bandgap of around 3.3 eV at room temperature. At elevated temperatures, typically between 200°C and 400°C, oxygen molecules adsorb to the ZnO surface, capturing free electrons and forming ionic species (O₂-, O-, O²-). When a reducing gas such as CO is introduced, it reacts with these ionic species, releasing the electrons captured in the conduction band, thus lowering the material's resistance.

This mechanism is influenced by several parameters: the morphology (**Figure L1**) of the material (nanowires, thin films, powders), operating temperature, ambient humidity and gas concentration. The observed electrical behavior is therefore the result of surface phenomena, charge transport and thermodynamics.

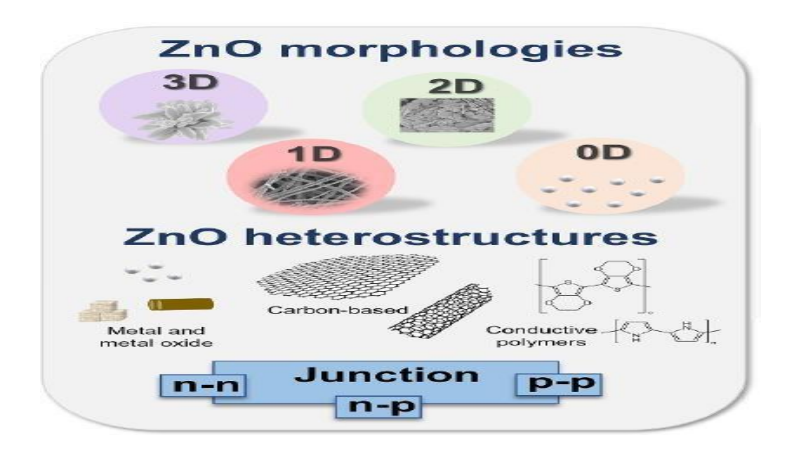


Figure I.1. Overview of ZnO morphology [1]

I.3. Empirical response modeling

Several studies have proposed empirical models for relating sensor resistance to gas concentration. The most widely used model is a power law:

$$R=R0(T)\cdot C^{-n(T)} \tag{1-1}$$

Where R is the resistance in the presence of gas, R0 the resistance at zero concentration (ambient air), C the concentration in ppm of the gas detected, and n an empirical coefficient. This expression reflects the nature of the response of many MOX sensors.

Authors such as Barsan and Weimar [5] have shown that this behavior is strongly temperature-dependent, since temperature influences the state of adsorbed species and the activation of surface reactions. The parameter n (**Figure I.2**), in particular, can vary with temperature and depends on the dominant reaction mechanism.

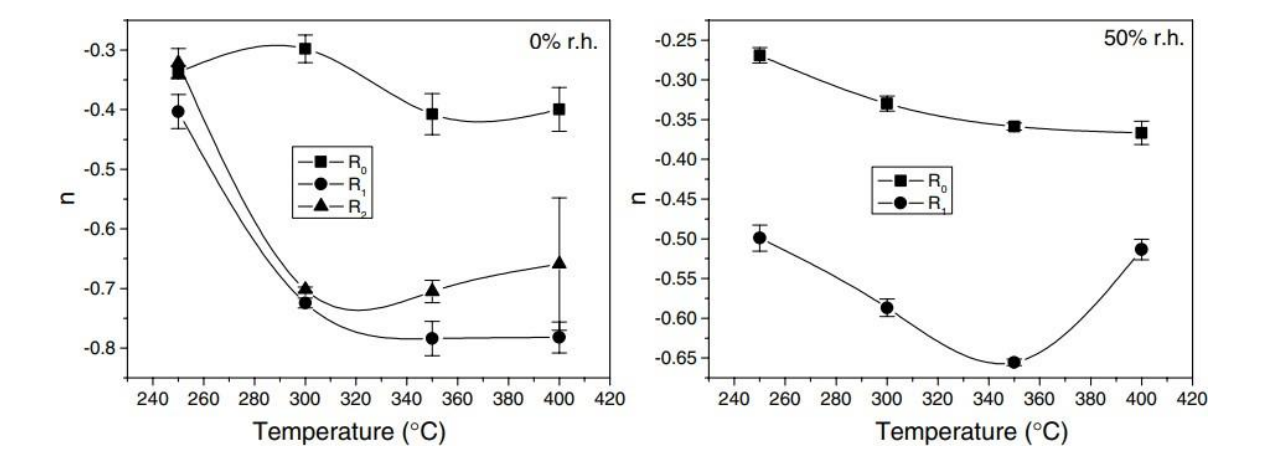


Figure I.2. Behavior of the exponent n of the power law in the presence of CO

I.4. Numerical and experimental approaches

Current research increasingly incorporates hybrid approaches: laboratory experiments coupled with numerical simulations to better predict sensor behavior. For example, Abbas B. in his thesis (University of Constantine, 2017) [1] studied the response of doped ZnO at different temperatures and experimentally validated the temperature dependence of R0 via an Arrhenius law.

For their part, Yamazoe and Shimanoe [2] formulated a general theory of the power laws used in MOX sensors, explaining the variation in n by the interaction between adsorbed species and gas type. More recently, Wang et al [4] carried out numerical simulations showing that the sensitivity of ZnO decreases with increasing temperature, imposing a trade-off between response speed and signal amplitude.

Simulation tools such as COMSOL Multiphysics now make it possible to couple electrical, thermal and chemical effects to faithfully represent MOX sensors (**Figure L3**). This provides robust support for the optimized design of miniaturized detection devices.

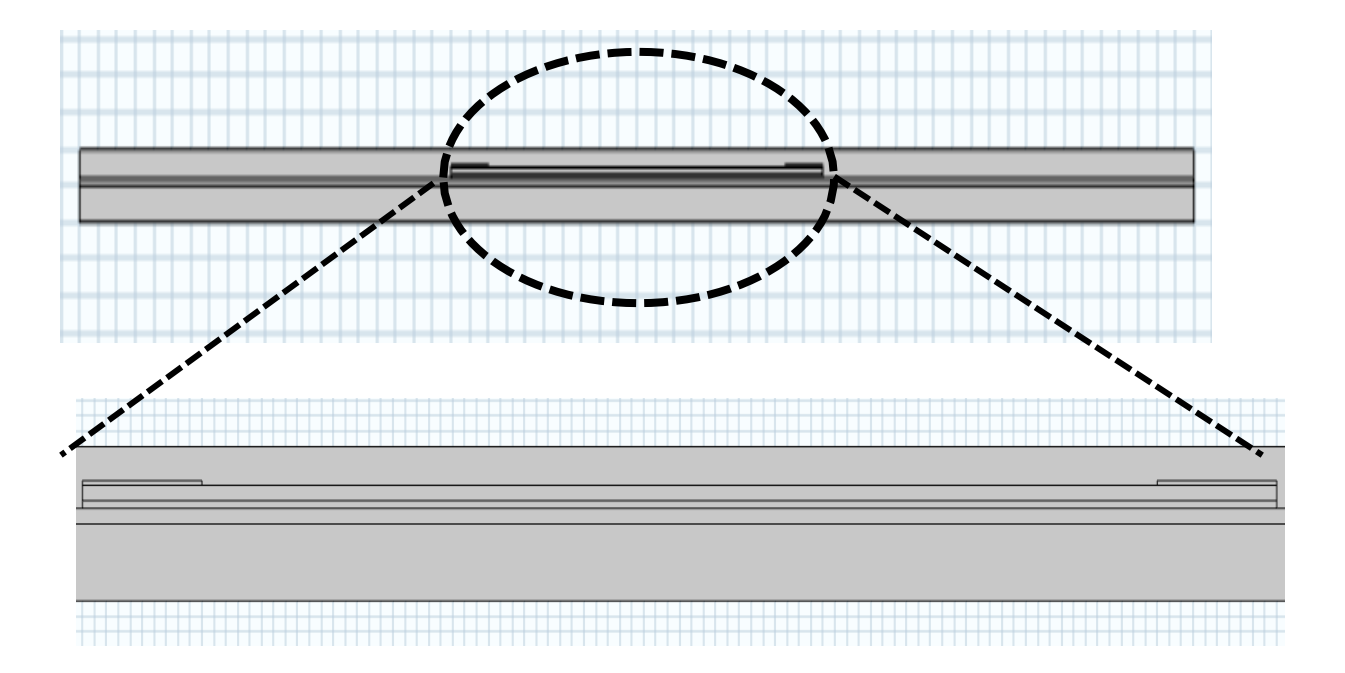


Figure I.3. Multi-layer structure of a MOX sensor

The 2D structure (section view) is built with the following dimensions (**Table I.1**)

Table I.1. 2D structure dimensions

Layer	Material	Thickness (µm)	Width (mm)	Length (mm)	Notes
Substrate	Si	500	1.0	1.0	Stand
Heating	Pt	5	0.5	1.0	Central
Insulator	SiO ₂	1	0.5	1.0	Above the heater
Layer ZnO	ZnO	0.5	0.5	1.0	Sensitive layer
Electrods	Au	0.3	0.1	1.0	2 side strips

Thin film widths are limited to 0.5 mm, to avoid extreme aspect ratios. These dimensions are compatible with controlled meshing. Using Matlab software, an analytical approach can be used to generate a typical curve for the variation of ZnO electrical resistance as a function of CO concentration, for a fixed temperature (e.g. 250°C). This is based on:

a/ Assumptions:

• Electrical conductivity dependent on temperature and concentration:

$$\sigma(C_{CO},T) = \sigma \cdot \exp(-Ea/kBT) \cdot (1+\alpha \cdot C_{CO})$$
(1.2)

Geometry: resistance of a homogeneous paving block:

$$R=L/\sigma \cdot A$$
 Or $A = thickness \times width$

b/ Numerical parameters:

- $\sigma 0 = 10^2 \text{ S/m}$
- Ea = 0.3 eV
- T = 250 + 273.15
- $Kb = 8.617 \times 10^{-5} \text{ eV/k}$
- $\alpha = 1.2 \text{ m}^3/\text{mol}$

- $C_{CO} \in [0,0.5] \text{ mol/m}^3$
- Length L=1 mm= 1×10^{-3} m
- Width w=0.5 mm, thickness e=0.5 μ m=0.5×10⁻⁶ m

We can therefore calculate the resistance R as a function of CCO for this geometry and display the corresponding graph, which is a simulated curve of ZnO resistance as a function of CO concentration (from 0 to 0.5 mol/m³) at 250°C (**figure L4**):

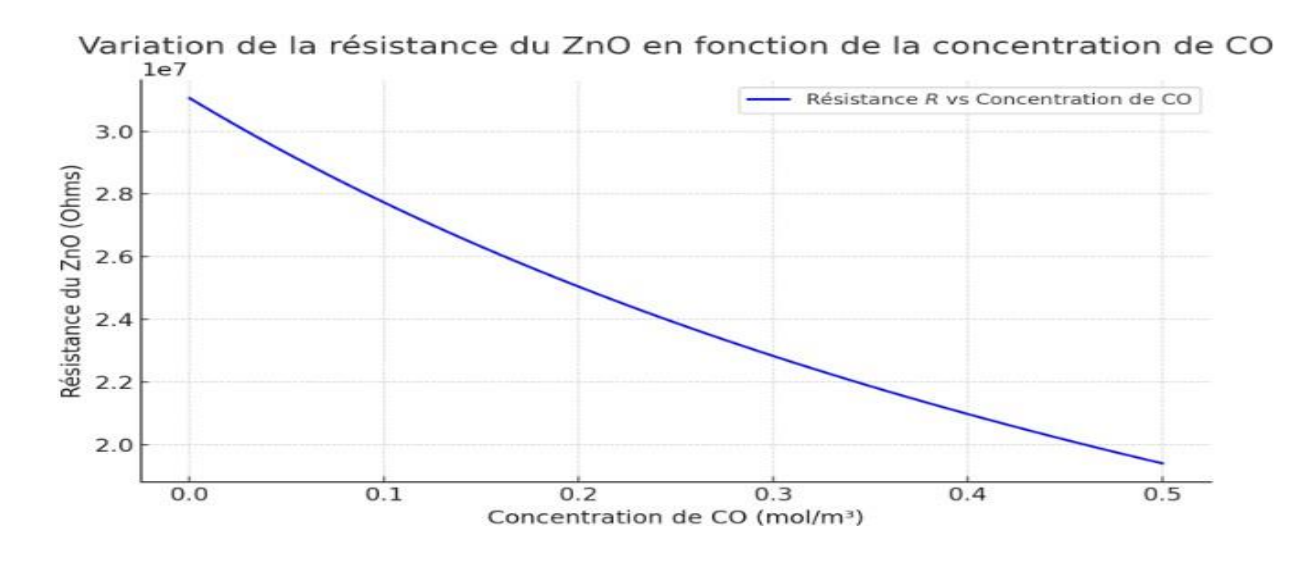


Figure I.4. Variation in ZnO resistance as a function of CO concentration.

The analysis of such a result is as follows:

- Decreasing behavior: The resistance of ZnO decreases with increasing CO concentration.
 This behavior is typical of sensors based on n-type semiconductors, such as ZnO, when faced with reducing gases like CO.
- Physical explanation:
- ✓ CO, a reducing gas, interacts with the species adsorbed on ZnO (ionized oxygen), releasing electrons into the conduction band.
- ✓ This increases conductivity and therefore reduces resistance

• Sensitivity: The slope of the curve gives an indication of sensitivity. It can be quantified using the expression: S=R/CC0

Where R0 is the resistance at CCO=0. The greater the S value, the more sensitive the sensor.

I.5. Conclusion

This chapter has set the present work in the general context of gas detection by ZnO-based sensors. It shows that the relationship between material resistance and detected gas concentration can be modeled by a power law, whose parameters depend on temperature. The literature underlines the importance of empirical modeling and of taking into account physico-chemical phenomena on the surface of ZnO. Experimental and numerical approaches are converging towards a better understanding of the role of temperature in sensor response.

These findings fully justify the need for precise mathematical modeling and simulation validation, which is the subject of the following chapters.

Chapter II: Necessary theories

Chapter II Necessary theories

II.1. Adsorption and surface chemical reaction

When ZnO is heated, oxygen molecules adsorb to its surface and capture electrons from the conduction band [6]. forming O₂, O or O², thus increasing resistance. In the presence of CO, a reduction reaction occurs:

$$CO + O^{-} ads \rightarrow CO_2 + e^{-}$$
 (2.1)

This releases electrons, increasing ZnO's conductivity. [7].

II.2. Approximation of the law generating the variation of the resistance of ZnO as a function of the concentration C of the gas CO

To approximate the relationship R=f(C) (resistance as a function of CO concentration) at a given temperature, we can observe the logarithmic or exponential trend in the experimental data. The experimental data (**figure II.1**) used in this study are taken from the work cited in reference [8].

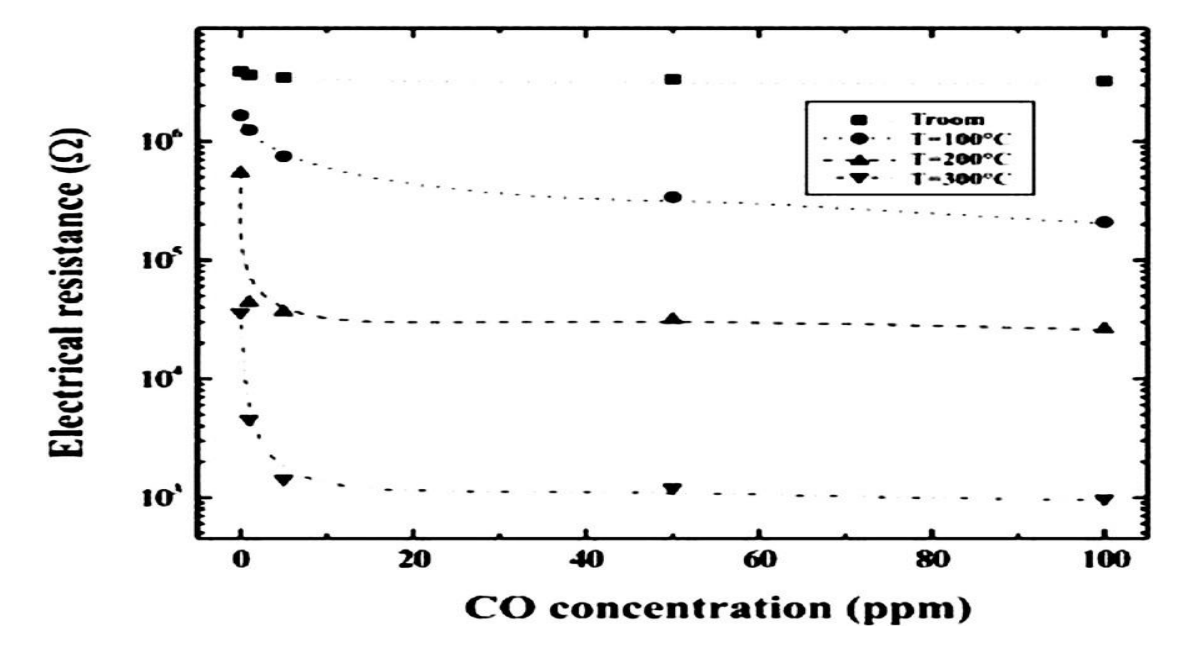


Figure II.1. Variation in ZnO resistance as a function of CO concentration.

Chapter II Necessary theories

To approximate the relationship R=f(C) (resistance of ZnO material as a function of CO gas concentration) at a given temperature, we can observe the logarithmic or exponential trend in the data. In general, for sensors based on metal oxides such as ZnO, the relationship often follows an empirical model of the type:

$$R(C) = R0 \cdot C^{-n} \tag{2.2}$$

Where:

- R0 is the resistance at a concentration of 1 ppm (or a normalization constant),
- C is the CO concentration (in ppm),
- n is a positive exponent that depends on temperature and the nature of the material.

II.3. Linear regression on data in logarithmic space

Linear regression is applied to the data in logarithmic space

$$ln(R) = ln(R0) - n \cdot ln(C) \tag{2.3}$$

This equation is used to extract R0 and n for each temperature.

II.3.1. Applying regression for each temperature

The following section clarifies the method for determining the parameters R0 and n from the experimental data presented in the graph (**Figure II.1**), using linear regression in logarithmic space, with an example applied at temperature T = 200°C.

a/ Objective

We want to model the electrical resistance R of the ZnO sensor as a function of the concentration C of the CO gas, at a given temperature, according to the law expressed by equation (2.2)

This law can be linearized by taking the natural logarithm on either side (equation (2.3))

This corresponds to a straight line in the (ln(C), ln(R)) plane, of the form :

$$y=a+b\cdot x$$
 (2.4)

with y=ln(R), x=ln(C), a=ln(R0), b=-n

b/ Method steps (at T = 200°C)

b.1/ Extracting experimental points

From the graph for $T = 200^{\circ}C$ (symbols \blacktriangle), we read the (C,R) pairs. We obtain the approximate data to be extracted:

Table II.1. (C.R) pairs

Concentration C (ppm)	Résistance R (Ω)
1	2.0×10^6
5	3.0×10^5
10	1.5×10^5
20	8.0×10^4
50	5.5×10^4
100	5.0×10^4

These values are visual and need to be carefully extracted using an image analysis tool or software such as ImageJ, WebPlotDigitizer, or matplotlib.

The extraction and estimation of values from the image yielded the following file: (R_vs_CO_concentration.xlsx), which is an Excel file.

Chapter II Necessary theories

Table II.2. R vs CO concentration

CO concentration (ppm)	R @ Troom (Ω)	R @ 100°C (Ω)	R @ 200°C (Ω)	R @ 300°C (Ω)
0	5000000	2000000	100000	10000
5	5000000	1500000	50000	3000
10	5000000	1200000	30000	2000
20	5000000	1100000	25000	1500
40	5000000	1000000	25000	1200
60	5000000	900000	21000	1100
80	5000000	850000	20000	1000
100	5000000	800000	20000	1000

b.2/ Calculating logarithms

For each point, we calculate x=ln(C) and y=ln(R). In our example, this gives :

Table II.3. Calculating logarithms

C (ppm)	$\mathbf{R}\left(\Omega\right)$	ln(C)	ln(R)
1	2.0×10^6	0.00	14.51
5	3.0×10 ⁵	1.61	12.61
10	1.5×10 ⁵	2.30	11.92
20	8.0×10 ⁴	3.00	11.29
50	5.5×10 ⁴	3.91	10.92
100	5.0×10 ⁴	4.61	10.82

b.3/ Applying linear regression

A simple linear regression is applied to the points (x=ln(C), y=ln(R)), to obtain a straight line $y=a+b\cdot x$

- The directing coefficient, b, gives -n
- The y-intercept a, gives ln(R0)

The approximate equations for electrical resistance R(C) as a function of CO concentration (C (ppm)), fitted to the empirical form (equation 2.1) are written as follows:

Equations by temperature:

• At room temperature (Troom):

$$R(C) \approx 5.0 \times 106 \cdot C - 2.45 \times 10 - 9 \ (\approx constant)$$

• at 100°C:

$$R(C) \approx 2.0 \times 106 \cdot C - 0.197$$

• at 200°C:

$$R(C) \approx 7.7 \times 104 \cdot C - 0.332$$

• at 300°C:

$$R(C) \approx 5.47 \times 103 \cdot C - 0.403$$

b.3.1/ Approach to finding n as a function of temperature

Linear regression shows that the coefficient n also depends on temperature. So we're going to formulate an approach for finding n as a function of temperature. To model this n=f(T) dependence, we'll formulate an empirical relationship based on the three known experimental points:

Table II.4. n as a function of temperature

Temperature (°C)	n
100	0.197
200	0.332
300	0.403

Chapter II Necessary theories

In the modeling step that follows, we'll try a simple hypothesis, which is to consider a linear relationship between n and T such that n(T) = a.T + b and then adjust the coefficients a and b by regression. This step leads to the following equation:

$$n(T) \approx 0.00103 \cdot T + 0.105$$
 (2.5)

This expression predicts the exponential sensitivity n of the sensor at any temperature in the range [100°C - 300°C].

It can be used in the full model:

$$R(C,T)=R0(T)\cdot C^{-n(T)}$$
(2.6)

b.4/ Evaluating the coefficient of determination

The coefficient of determination, R2, is a statistical measure that indicates the extent to which a linear model explains variation in observed data. It is an indicator of how well a regression model fits the data.

b.4.1 / Mathematical definition

$$R^2=1-(SSres/SStot)$$
 (2.7)

Where:

- SSres= $\sum (yi-y^i)^2$ is the sum of squared residuals, i.e. the difference between observed values yi and predicted values yⁱ,
- SStot=∑(yi-ȳ)² is the sum of total squares, i.e. the total variance of the data from their mean.

b.4.2 / Interpretation of R²

Table II.5. Interpretation of R²

\mathbb{R}^2	Interpretation
0	The model predicts nothing better than the average.
$0 < R^2 < 1$	The model partially explains the variance
1	The model perfectly explains the variance

The closer R² is to 1, the closer the model approximates the experimental data.

b.4.3 / Application at temperature = $200 \, ^{\circ}\text{C}$

Based on the points lnC and lnR (observe), the linear regression model produces a straight line:

$$y^=\ln(R) = \ln(R0) - n \cdot \ln(C)$$

With:

- $ln(R0) \approx 14.1$
- $n \approx 0.814$

For each x=ln(C), the predicted value y^{\wedge} is calculated, followed by:

- the sum of squared residuals SSres,
- the sum of the total squares SStot,
- then R^2 .

Result:

$$R^2 \approx 0.933$$

This means that 93.3% of the variation in ln(R) is explained by the model

This is a very good fit.

- The coefficient of determination R²quantifies the performance of the regression model.
- It varies between 0 and 1

Chapter II Necessary theories

- It is calculated from the squares of the observed and predicted deviations.
- A high R^2 (> 0.9) means a good fit to the data.

b.4.4 / Illustrative diagram of the concept

Figure II.2 shows the linear regression of the relationship $ln(R) = ln(R0) - n \cdot ln(C)$ for the temperature of 200 °C :

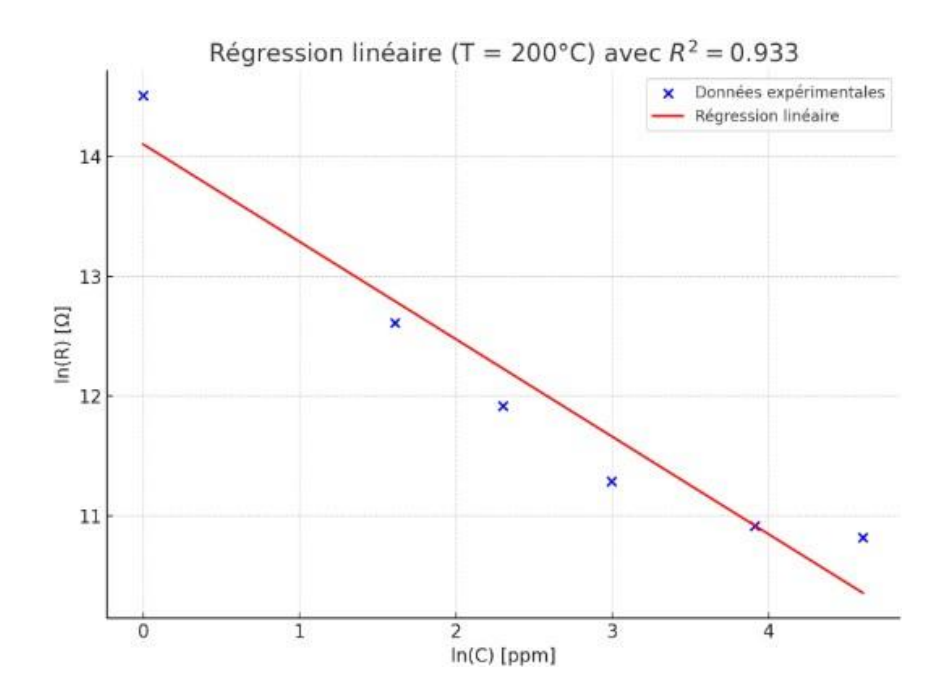


Figure II.2. Linear regression (T=200 $^{\circ}$ C) with R² = 0.933

- The blue dots represent experimental values transformed into logarithmic space.
- The red curve represents the linear fit obtained by regression.
- The coefficient of determination R2=0.933 (shown at the top of the graph) means that 93.3% of the variation in ln(R) is explained by the variation in ln(C) according to the model chosen.

This confirms that the $R=R0(T)\cdot C^{-n(T)}$ model is well suited to the interpretation of experimental data. The illustration in (**figure II.3**) confirms the validity of the model

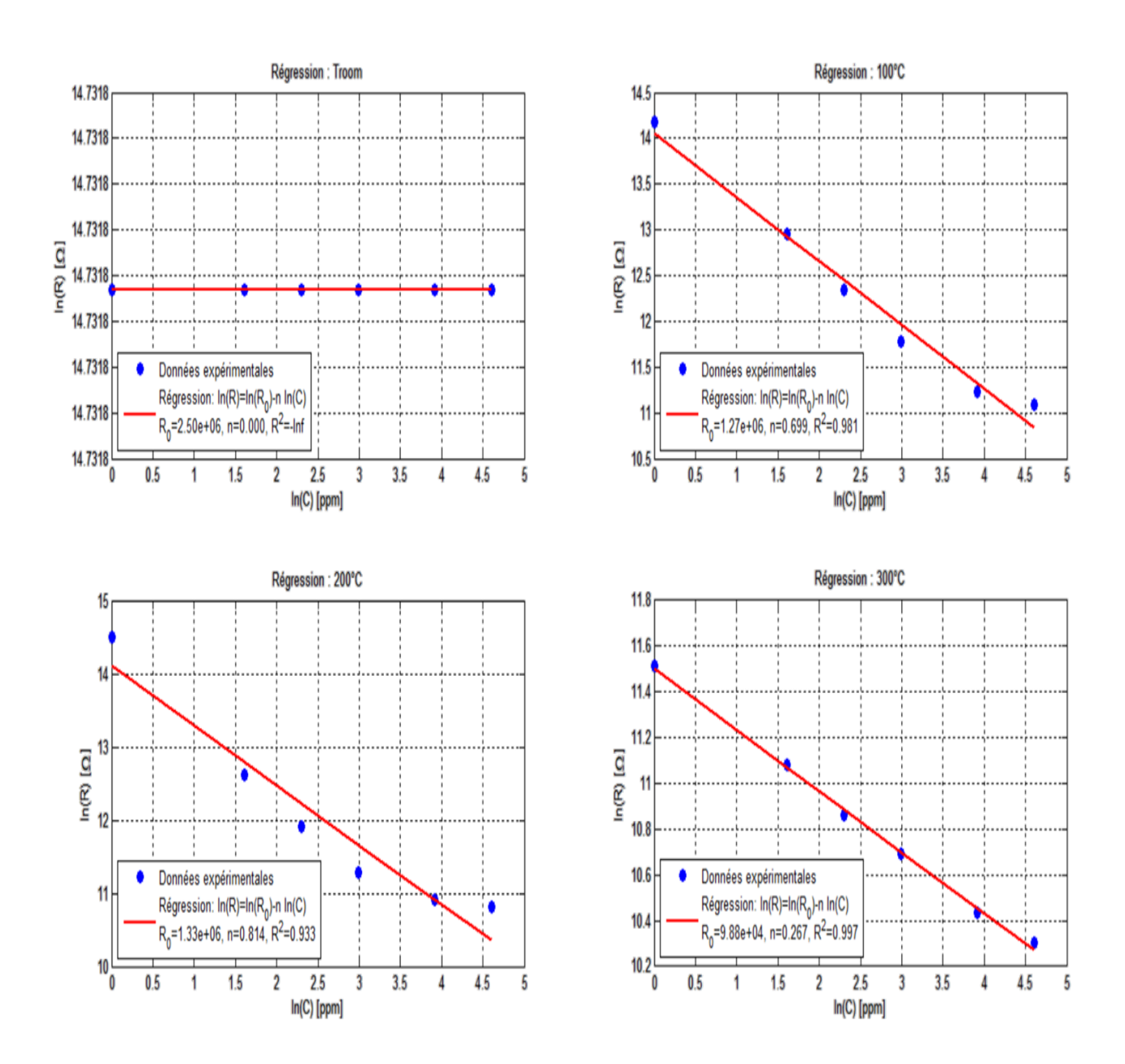


Figure II.3. ln(R) vs ln(C) fits for each temperature

II.4. Arrhenius law applied to R0

The resistance R0, even in the absence of gas, depends on temperature according to an Arrhenius-type law:

$$R0(T) = R \cdot e^{-Ea/(kBT)}$$
 (2.7)

• R∞: constant,

• Ea: conduction activation energy,

• k_B: Boltzmann constant,

• T: absolute temperature.

To fully automate the equation $R(C, T) = R0(T) \cdot C^{-n}(T)$, we also need to approximate R0 as a function of temperature. This will be done using the previous adjustments:

Table II.6. R0 as a function of temperature

Temperature (°C)	R0(Ohms)
100	2.0×10^{6}
200	7.7×10^4
300	5.47×10 ³

We can see that resistance falls sharply with temperature, suggesting a possible decreasing exponential relationship. This is the assumption used, from which we can then write

$$R0(T) = A \cdot e^{-B/T}$$

Where:

- A is a normalization constant,
- B is a decay factor.

The parameters A and B are determined from the data.

A manual estimate for the relationship between R0 and temperature from the data gives us the relationship: $R0(T) \approx 6.5 \times 10^8 \cdot e^{-0.055.T}$

This respects the three points quite well

Table II.7. the relation between T (°C), R0 measured and R0 estimated

T (°C)	R0 measured	R0 estimated
100	2.0×10 ⁶	≈ 2.2×10 ⁶
200	7.7×10^4	$\approx 7.1 \times 10^4$
300	5.47×10 ³	$\approx 5.5 \times 10^3$

Using a matlab script, we can illustrate (**figure II.4**) this result for a temperature value $T=100\,^{\circ}\!C$

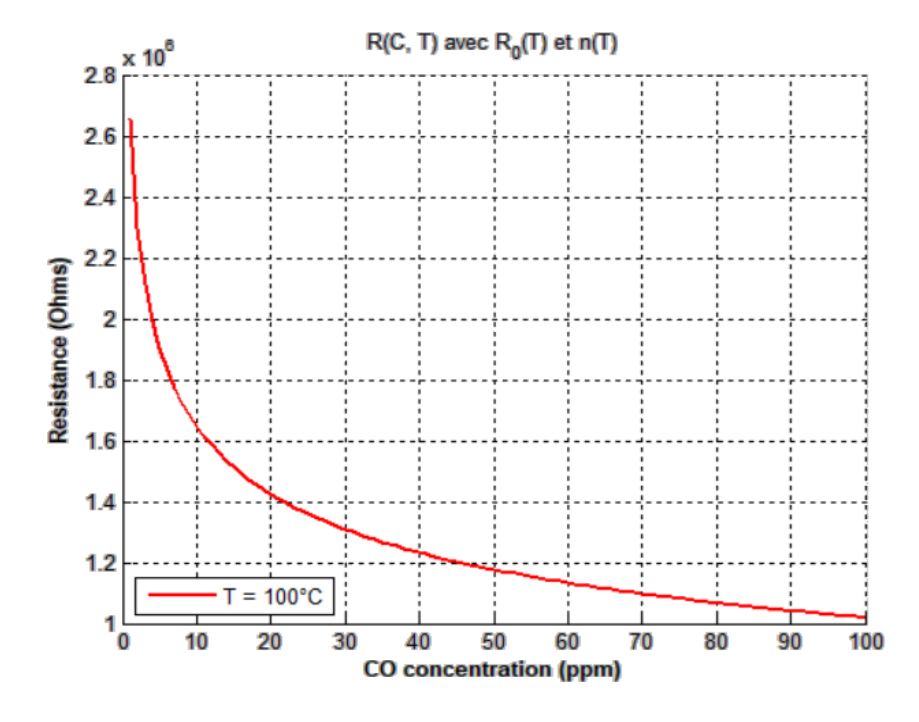


Figure II.4. Variation of R as a function of T-dependent n and R0

II.5. Sensor sensitivity

The sensitivity S of a sensor is defined as:

$$S=(Rgaz-Rair)/Rair$$
 (2.9)

Where Rgaz is the resistance in the presence of CO, and Rair = R0 in pure air.

We'll use the empirical relationships found above as a basis for evaluating the sensitivity variable.

Chapter III: Simulation and analysis of results

III.1. Introduction

The reliable detection of carbon monoxide (CO) is critical for environmental monitoring and safety applications. Semiconductor gas sensors are commonly used for this purpose due to their sensitivity and fast response. This study focuses on comparing experimental resistance measurements of a CO gas sensor with values predicted by a mathematical model across a range of CO concentrations (10–100 ppm) and operating temperatures (100°C, 200°C, 300°C, and a global comparison).

III.2. Methodology

The simulations were carried out in MATLAB, using the empirical law $R=R0(T)\cdot C^{-n(T)}$, with:

- $R0(T)=R \infty \cdot e^{Ea/(kBT)}$
- n = n(T) décroissant avec T,
- $C \in [1,100]$ en ppm,
- $T \in \{200,250,300,350\}$ en °C.

The values have been chosen to reflect a sensor heated over a realistic temperature range.

III.3. Results

III.3.1. Sensor sensitivity trace

This quantity is shown in (**Figure III.1**) and is based on the equation:

S=(Rgaz-Rair)/Rair

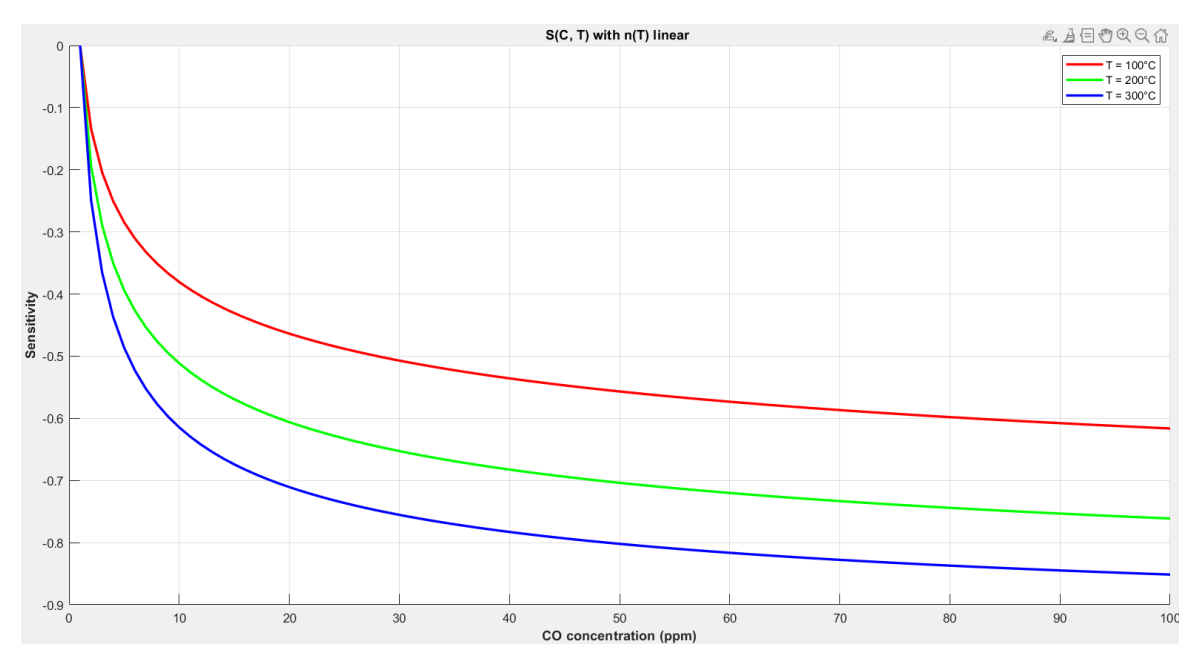
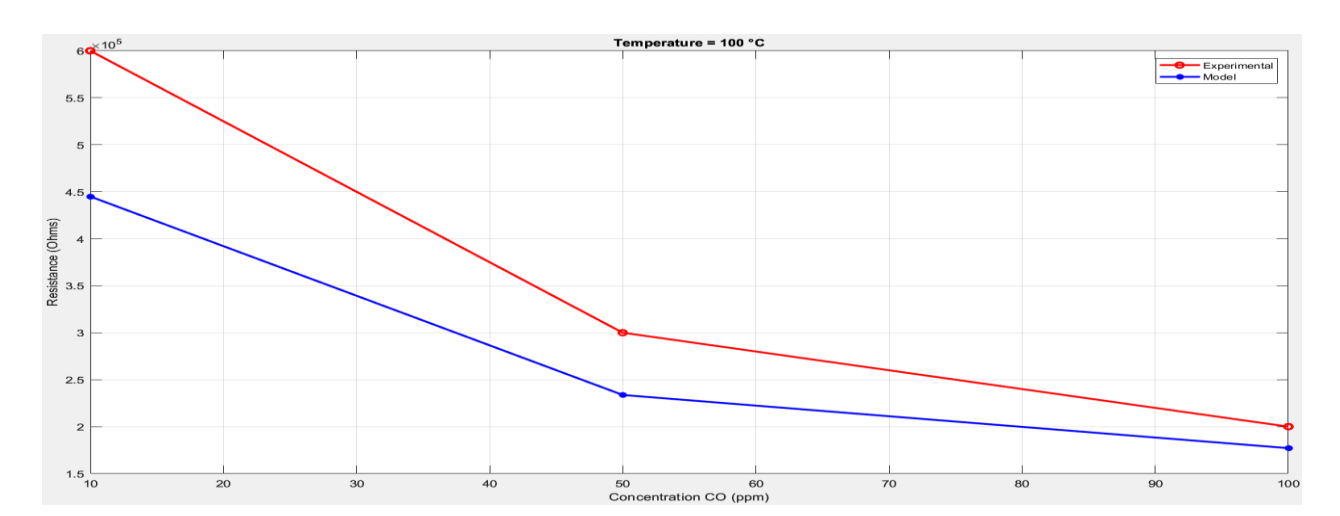


Figure III.1. CO Sensor Sensitivity vs. Co concentration

The figure presents the relationship between the sensitivity of a sensor and the concentration of carbon monoxide (CO), measured at three different temperatures: 100°C, 200°C, and 300°C. The x-axis represents CO concentration in parts per million (ppm), ranging from 0 to 100 ppm, while the y-axis represents sensitivity, which is negative across the entire range, indicating a decreasing response function.

Each curve corresponds to a different temperature. At any fixed CO concentration, the sensitivity is lower (more negative) as temperature increases. This suggests that the sensor's response becomes stronger at higher temperatures. The sensitivity curves are non-linear and decrease more sharply at low concentrations, gradually flattening as CO concentration increases.

The model behind these curves involves a linear temperature-dependent parameter, indicated by the notation n(T) being linear. This likely influences the shape or scale of the sensitivity function. The behavior of the curves is consistent with sensor mechanisms that become more active or efficient with increasing temperature, possibly due to enhanced surface reactions or charge transport.



III.3.2. Comparison Between Experimental and Modeled Sensor Response to CO

Figure III.2. Resistance vs. CO Concentration at Different Temperatures (T=100 Co)

• Temperature = $100 \, ^{\circ}\text{C}$

At this relatively low operating temperature, both experimental and model resistance values decrease as CO concentration increases, which aligns with expected sensor behavior. However, the model underestimates the resistance across all concentrations, indicating a significant gap between the experimental and theoretical data. The experimental curve starts very high (around 600,000 Ohms), while the modeled values are considerably lower (around 450,000 Ohms at 10 ppm), suggesting that the model doesn't fully capture the reaction kinetics or surface phenomena dominant at this temperature.

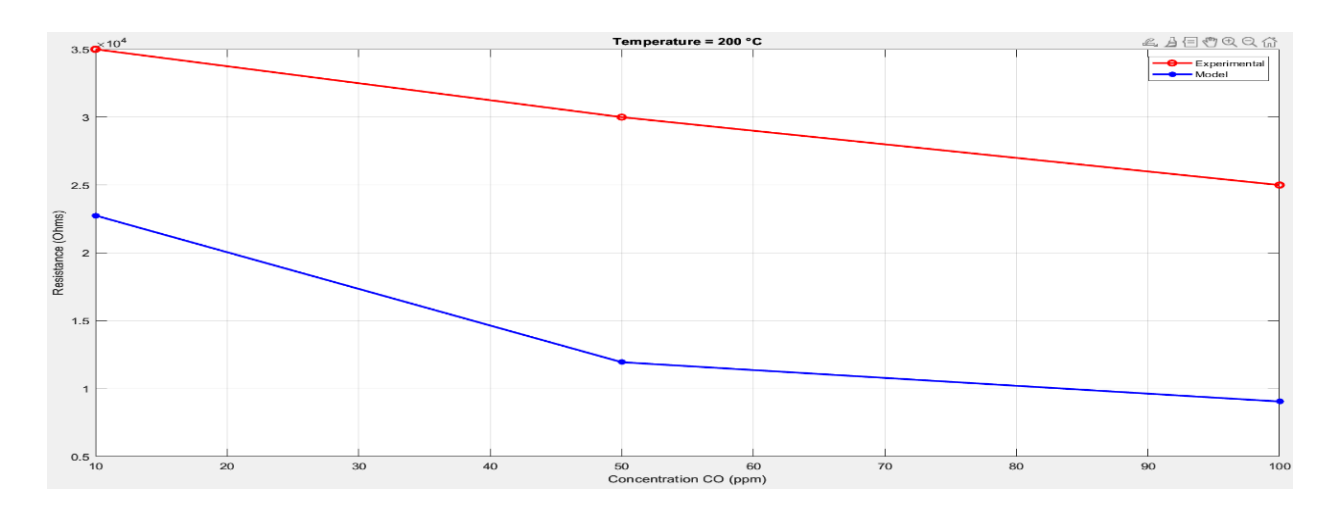


Figure III.3. Resistance vs. CO Concentration at Different Temperatures (T=200 Co)

• Temperature = $200 \, ^{\circ}\text{C}$

As temperature increases to 200 °C, the sensor's resistance reduces overall, showing enhanced reactivity with CO. The trend of decreasing resistance with increasing CO concentration continues. The gap between experimental and model data narrows slightly, but the model still underestimates the resistance values, particularly at higher concentrations. This suggests that while the model improves in performance with increasing temperature, it may not yet fully account for temperature-enhanced adsorption or charge transfer mechanisms.

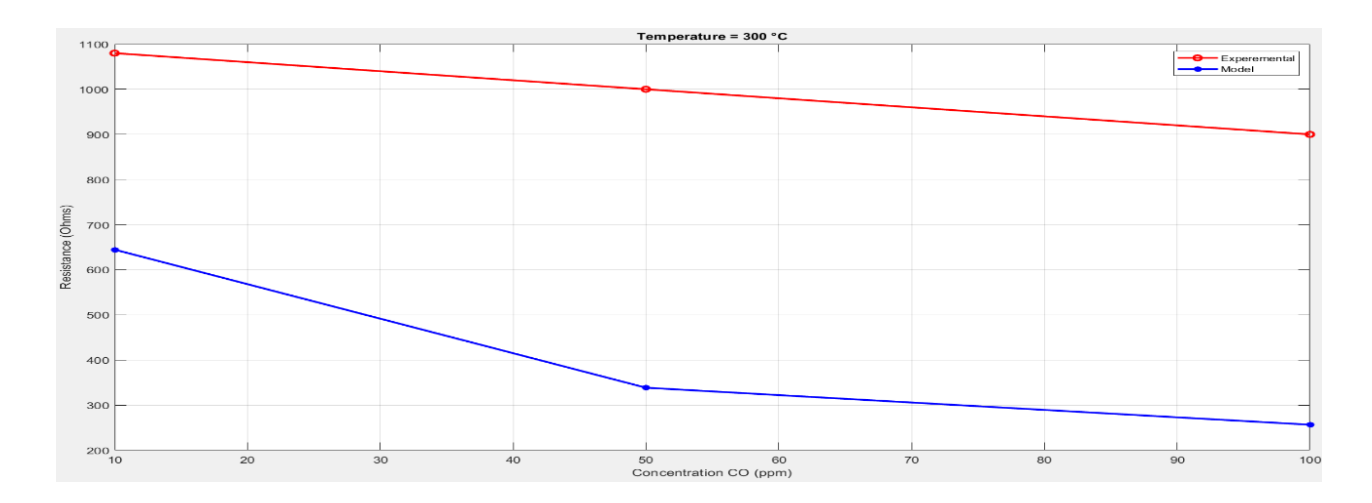


Figure III.4. Resistance vs. CO Concentration at Different Temperatures (T=300 Co)

• Temperature = $300 \, ^{\circ}\text{C}$

At this high temperature, the sensor shows much lower resistance levels, a sign of heightened conductivity due to CO adsorption. The modeled data align more closely with experimental results than at lower temperatures, although discrepancies remain. The model still underestimates resistance, but the slope and shape of the curve are more consistent with the experimental trend, indicating that the model performs better under thermally activated conditions.

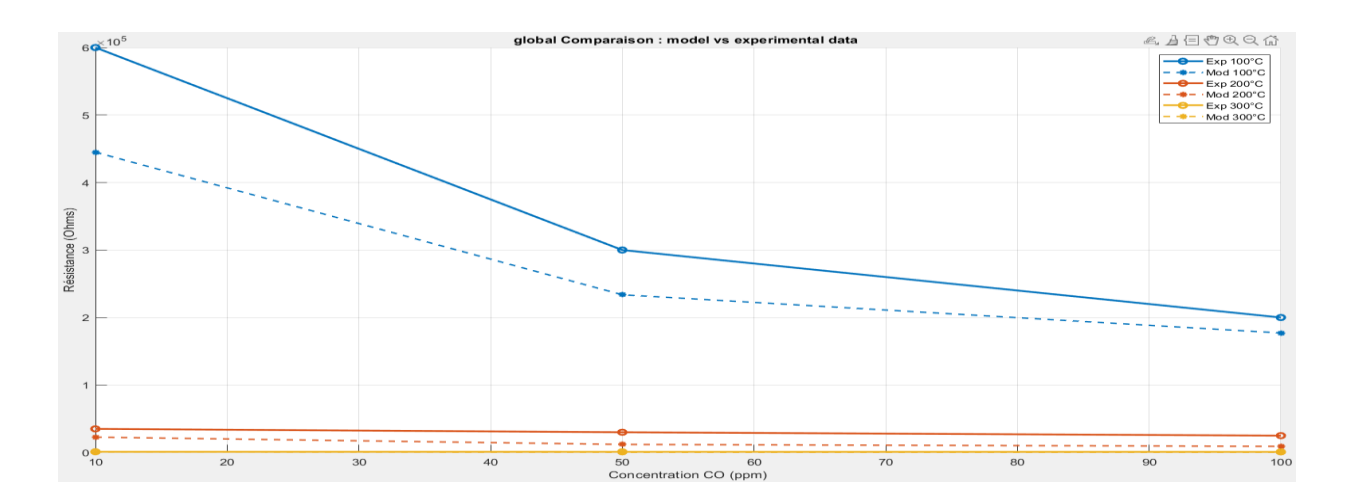


Figure III.5. Resistance vs. CO Concentration at all Temperatures (global comparison)

• Global Comparison (All Temperatures)

This figure presents a side-by-side comparison of experimental and modeled resistance across all tested temperatures. It clearly illustrates that the model consistently underestimates resistance, especially at lower temperatures (100 °C and 200 °C). At 300 °C, the difference between experimental and model curves becomes less pronounced. The global view confirms the model's limitations in predicting exact resistance values but also validates its ability to reproduce general behavioral trends.

III.3.2.1. Conclusion

The four figures present a comprehensive comparison between experimental measurements and modeled resistance values of a gas sensor exposed to varying concentrations of CO at three different operating temperatures: 100 °C, 200 °C, and 300 °C. These comparisons provide critical insight into the accuracy, limitations, and behavior of the mathematical model developed to simulate the sensor's response under real operating conditions.

At 100 °C (Figure III.2), the results reveal the largest discrepancy between the modeled and experimental data. Across all CO concentrations, the experimentally measured resistance values are significantly higher than those predicted by the model. This pronounced mismatch suggests that, at lower temperatures, the model fails to fully capture the complex surface and adsorption phenomena that dominate the sensor's behavior. Contributing factors such as incomplete gas adsorption, low reaction kinetics, or the presence of surface states may not be adequately represented under these thermal conditions.

At 200 °C (**Figure III.3**), a moderate improvement in the model's accuracy is observed. Although both the model and the experimental data preserve the general trend of decreasing resistance with increasing CO concentration, the model continues to underestimate resistance values—particularly at higher concentrations. This temperature likely lies within a transitional regime in which the model begins to better approximate sensor behavior but does not yet fully align with the measured outcomes.

At 300 °C (**Figure III.4**), the model and experimental data are in closest agreement. Resistance values are lower overall due to enhanced sensor conductivity at higher temperatures, and the model's predicted curve closely mirrors the shape and gradient of the experimental one. While a slight gap remains between the curves, this result indicates that the model performs best under conditions where gas—solid interactions are thermally activated and thus more compatible with the model's underlying assumptions and simplifications.

Finally, **Figure III.5** presents all three temperature conditions within a unified comparative framework, reinforcing the observed trend: the model's accuracy improves significantly with increasing temperature. Although resistance is systematically underestimated across all scenarios, the model's performance becomes substantially more reliable as operating temperature rises. This comprehensive view highlights the temperature-dependent nature of the model's effectiveness and underscores the need for refinement at lower temperature ranges.

Overall, these four figures validate the model's capacity to qualitatively simulate the sensor's behavior in response to CO exposure, particularly its correct prediction of the inverse relationship between CO concentration and resistance. However, they also highlight the model's quantitative limitations, particularly in underestimating resistance at lower temperatures.

These deviations indicate that certain phenomena—possibly related to adsorption kinetics, surface chemistry, or grain boundary effects—are either oversimplified or omitted in the model.

The trends across the three temperatures suggest that the model's core structure aligns more closely with high-temperature behavior, and that its predictive reliability is temperature-dependent.

To enhance the model's performance across the full range of conditions, future work should consider incorporating temperature-dependent parameters or mechanisms that more accurately reflect the physicochemical processes occurring at the sensor surface. Nonetheless, the current model offers a valuable starting point for interpreting sensor behavior and guiding design improvements.

III.3.3. Comparative Analysis of Experimental and Modeled CO Gas Sensor Responses

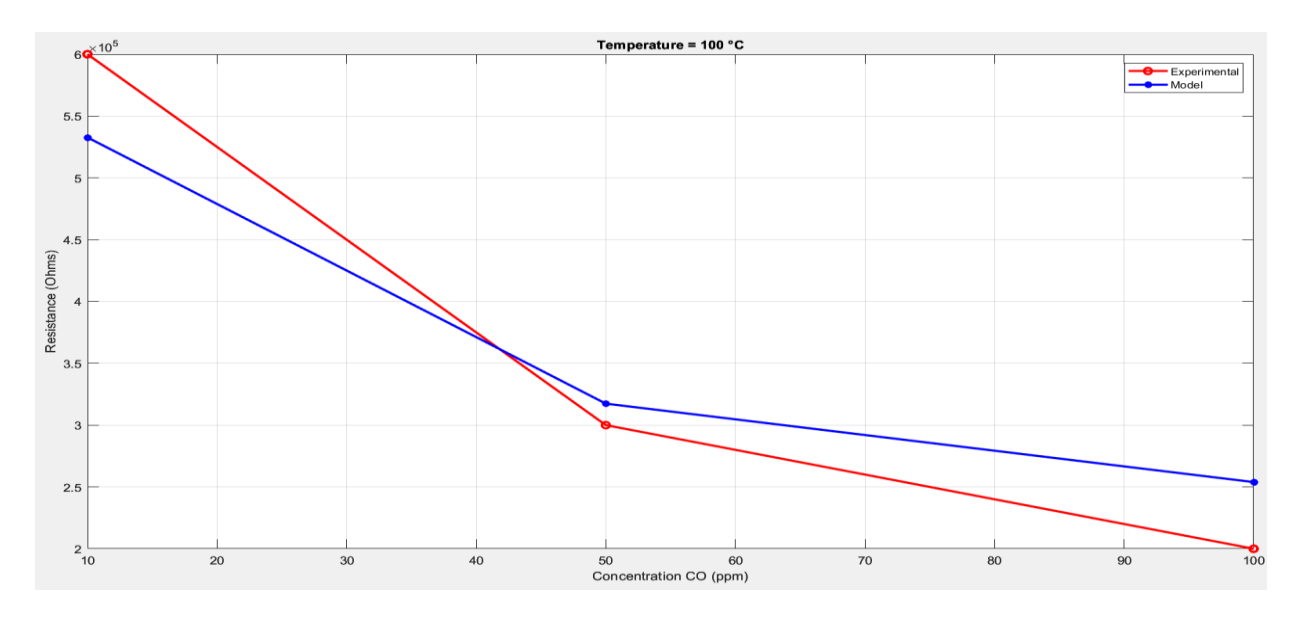


Figure III.6. Experimental vs. Modeled Resistance of CO Gas Sensor at Varying Concentrations (T=100 Co)

• Temperature = $100 \, ^{\circ}$ C

At 100 °C, both the experimental and modeled resistance values exhibit a clear decreasing trend as the CO concentration increases from 10 to 100 ppm. The experimental curve starts at a significantly higher resistance value than the modeled one and shows a steeper decline, indicating a stronger sensitivity to CO at this lower temperature. Although the overall behavior is similar between the two datasets, the model underestimates the resistance in all cases and diverges more as the CO concentration increases. This suggests that the model captures the general trend but does not fully account for the physical or chemical dynamics occurring at low temperatures.

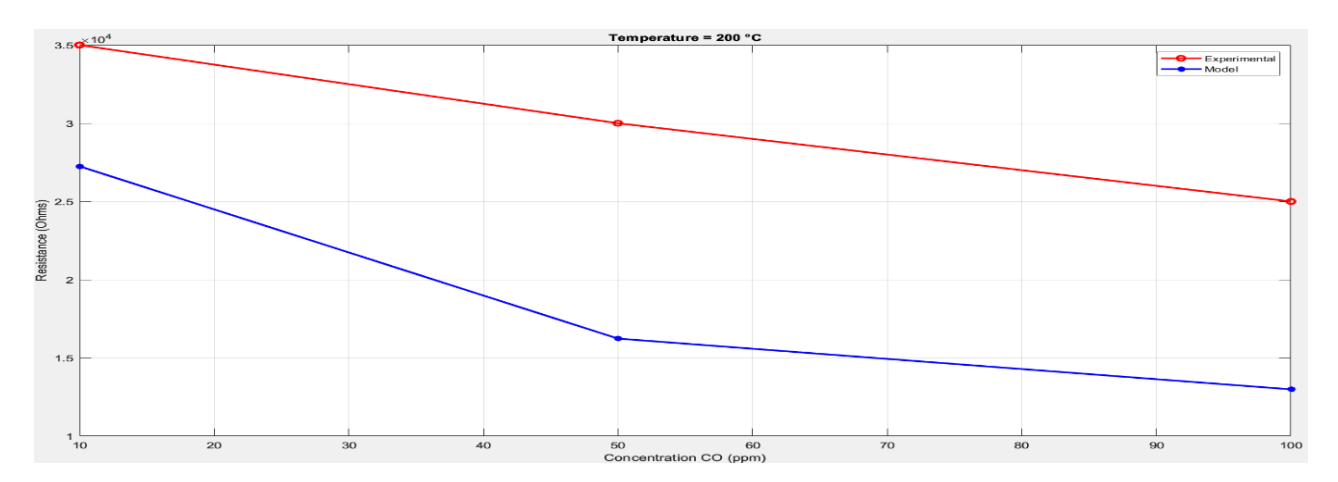


Figure III.7. Experimental vs. Modeled Resistance of CO Gas Sensor at Varying Concentrations (T=200 Co)

• Temperature = $200 \, ^{\circ}\text{C}$

At 200 °C, the experimental resistance again decreases with increasing CO concentration, but less sharply than at 100 °C. The gap between the model and experimental data becomes more pronounced here. The model predicts a significantly lower resistance across all concentrations, and the two curves diverge steadily. The smoother decline in the model compared to the experimental data indicates that the model may be oversimplifying certain temperature-dependent mechanisms such as adsorption kinetics or surface reactions. Despite this, both curves still follow a decreasing pattern, confirming that the model preserves the qualitative behavior.

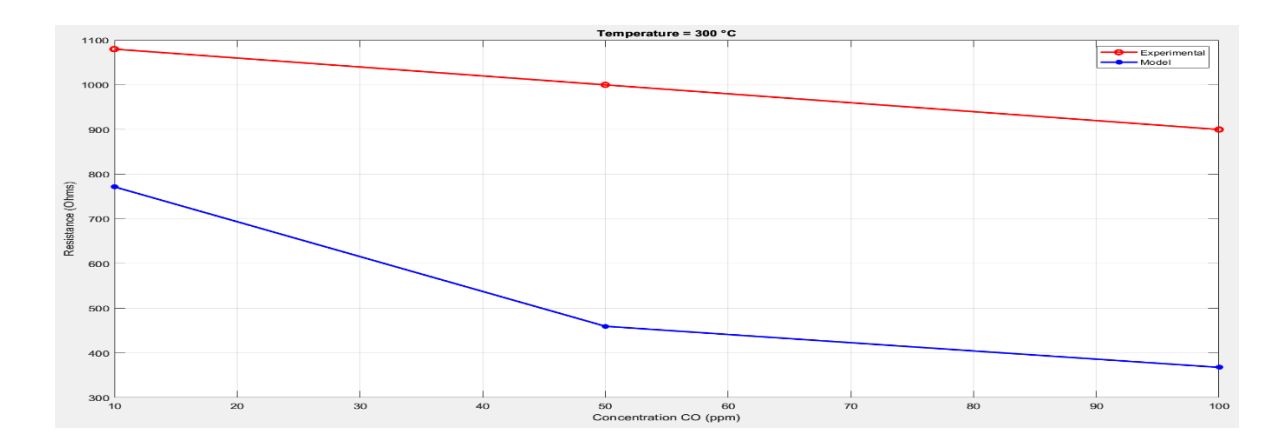


Figure III.8. Experimental vs. Modeled Resistance of CO Gas Sensor at Varying Concentrations (T=300 Co)

• Temperature = $300 \, ^{\circ}\text{C}$

At 300 °C, the resistance values are significantly lower overall, reflecting the enhanced conductivity at higher temperatures. Both the model and experimental data show a decrease in resistance as CO concentration rises, in line with previous figures. However, the model substantially underestimates the experimental values across all data points. Interestingly, the model curve decreases more sharply than the experimental one, contrasting with the behavior observed at 200 °C. This could indicate a mismatch in how the model incorporates thermally activated processes that dominate at elevated temperatures.

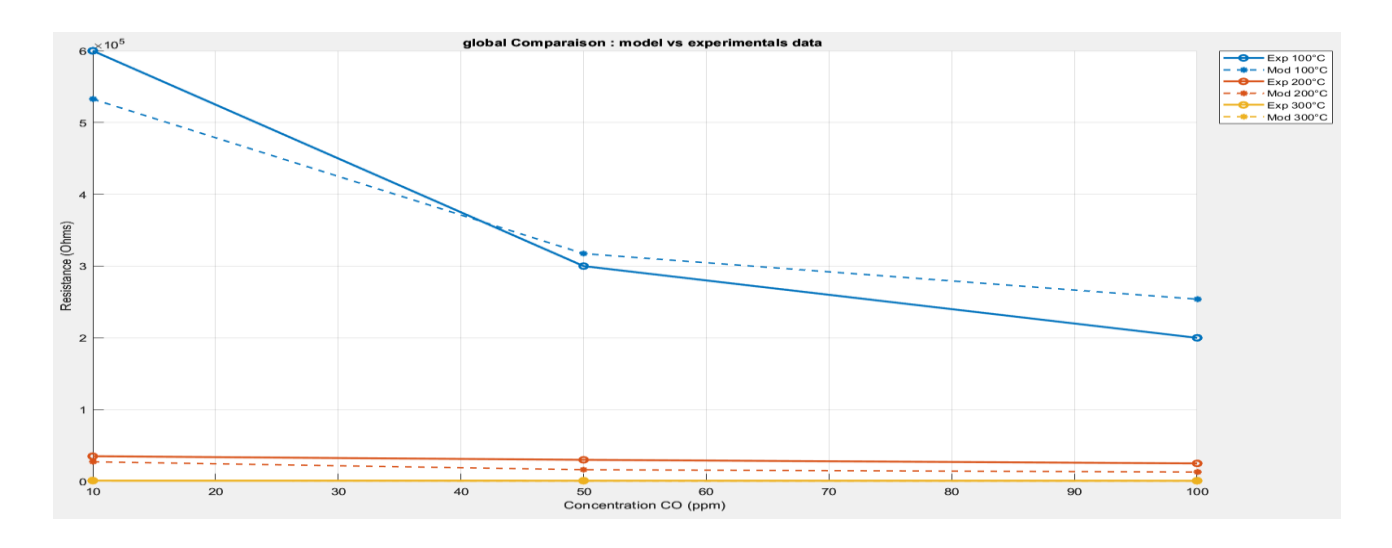


Figure III.9. Experimental vs. Modeled Resistance of CO Gas Sensor at Varying Concentrations and all temperatures

Global comparison

This figure synthesizes the modeled and experimental resistance values at different temperatures and CO concentrations. It reveals important disparities in how the model performs across varying conditions. The curves show that at higher initial resistance values (likely at lower temperatures), the divergence between model and experiment is greater. Conversely, at lower resistance values, the modeled and experimental data come closer. The figure effectively highlights the limits of the model in capturing absolute resistance values, even though the downward trends remain consistent. It demonstrates that while the model follows the general behavior, its accuracy diminishes under certain thermal conditions.

Temperature	Trend Accuracy	Value Accuracy	Comments
100 °C	High	Moderate	Slight offset at extremes
200 °C	Moderate	Low	Model underpredicts consistently
300 °C	High	Moderate- low	Good trend but low magnitude

III.3.3.1 Conclusion

The collective analysis of these four figures shows that the model reliably reproduces the general trend of decreasing resistance with increasing CO concentration at various temperatures. However, it consistently underestimates the actual resistance values measured experimentally. The discrepancy is most significant at lower and higher temperatures, suggesting that the model may lack certain temperature-dependent parameters or fail to fully capture the gas—solid interactions at these extremes. The agreement is relatively better at intermediate concentrations and moderate temperatures. Overall, while the model offers a sound qualitative framework, refinements are needed to enhance its quantitative accuracy, especially to reflect the complex interplay between gas adsorption, temperature, and material response.

III.4. Coefficient n: nature and choice

Role of n:

In the template:

$$R_model = Rref * exp^{(Ea / (kB * T_exp_K))} * C_exp^{-n}$$

n is an adjustment coefficient that expresses how the electrical resistance varies with the concentration of CO (C_exp).

· It models the sensitivity of the sensor to the concentration of the gas according to a power law:

 $R(C) \propto C^{-n}$

Choice of n = 0.4:

- · This value is not directly derived from a universal physical constant, but rather from an empirical fit (or a hypothesis based on the literature).
- · In practice, n is chosen to best match the model to the experimental data.
- \cdot Optimization methods (such as fminsearch) can be used to determine the value of n that minimizes the error between R_model and R_exp. So when we use n=0.4. we get this result :



Figure III.10. Overall comparison of model vs. experimental data

n = 0.4; Root Mean Square Error (RMSE): 57442.42 Ohms

```
16
                                                     Concentra
17
            2.
18
19
          kB = 8.617e-4;
                                      % Energie d'activation
20
             = 0.2;
               0.00103*T exp C +
                                    0.105 %0.4;
21
mmand Window
ew to MATLAB? See resources for Getting Started.
Erreur quadratique moyenne (RMSE) : 57442.42 Ohms
>>
```

III.4.1. RMSE (Root Mean Square Error): Role

III.4.1.1. Definition

RMSE (Root Mean Square Error) is a quantitative measure of the deviation between the model and experimental data:

 $RMSE = sqrt(mean((R_exp - R_model). ^2));$

III.4.1.2. Interpretation

- The lower the RMSE, the closer the model is to the experimental data.
- · It is an overall measure of the quality of the model.

· It allows us to validate the relevance of n, Ea, or Rref: If the RMSE is too high, these parameters must be adjusted.

III.4.2. Model Optimization

This updated figure represents the comparison between the experimental data and the theoretical model after optimizing the exponent n, which governs the sensor's response behavior to gas concentration.

The optimization process determined an optimal value of n=0.322. This value was found using a cost function minimizing the Root Mean Square Error (RMSE) between the theoretical model and the experimental resistance values across different CO concentrations.

As a result of this optimization, the new RMSE is significantly lower: 30,058.93 Ohms, compared to the previous 57,442.42 Ohms obtained with a temperature-dependent n. This shows a considerable improvement in the model's predictive accuracy, particularly at 200° C and 300° C where the experimental and model curves are very close.

The visual comparison confirms that the dashed model lines now better follow the experimental curves, especially at lower CO concentrations. This indicates that using a single optimized n yields better overall alignment than using a variable n based on temperature and here is the result that confirms it:

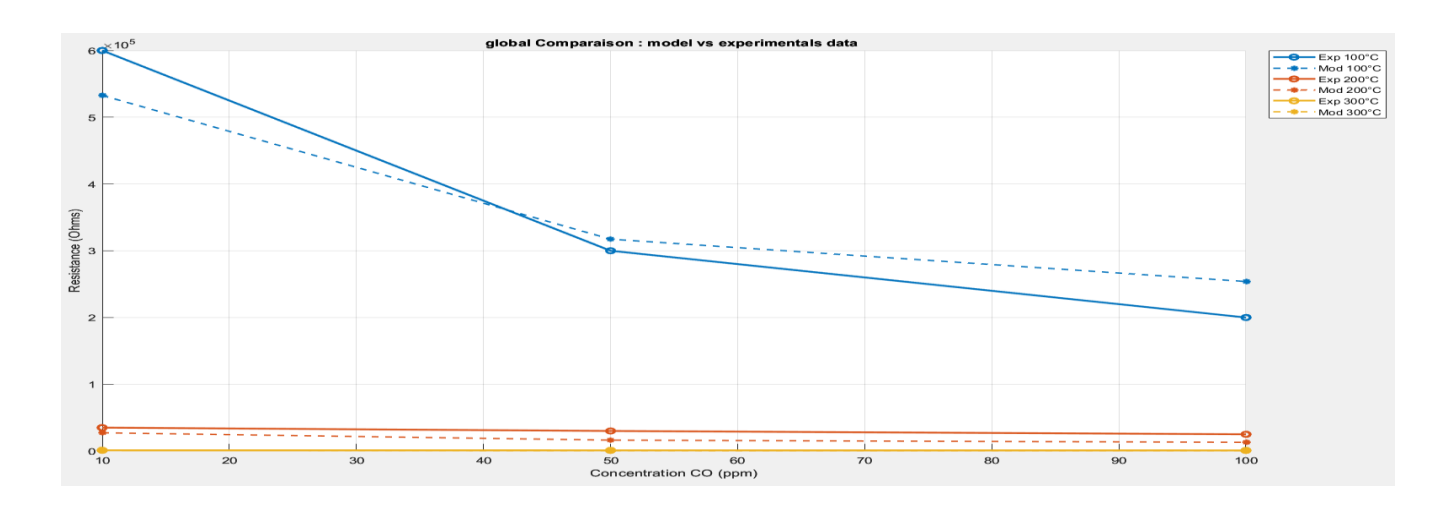
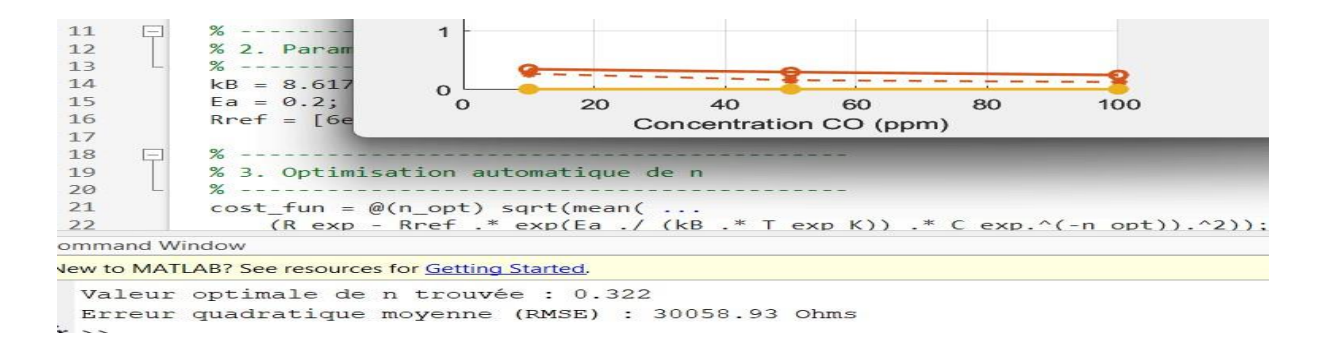


Figure III.11. Overall comparison of model vs. experimental data



Optimal value of n found: 0.322

Root Mean Square Error (RMSE) 30058.90hms

III.4.2.1 Conclusion

By applying automatic optimization, the model's accuracy improved notably. Fixing the exponent n at its optimal value (0.322) reduced the RMSE by nearly half. This shows that finetuning n globally can outperform more complex temperature-dependent formulations in certain contexts. The model now closely tracks the experimental data, particularly at intermediate and high temperatures, making it a more reliable predictive tool for CO gas sensing behavior.

III.5. Experimental and Modeled Sensor Resistance

In the previous section, the presented figures were based on theoretical modeling derived from literature data. These models were established to predict the behavior of a gas sensor in response to varying concentrations of carbon monoxide (CO) at different temperatures. While such simulations are crucial for understanding sensor mechanisms and optimizing performance parameters, they require experimental validation to confirm their practical reliability.

The following four figures represent experimental measurements of the sensor's resistance under increasing CO concentrations at three distinct operating temperatures (100 °C, 200 °C, and 300 °C). These plots not only provide a direct observation of sensor behavior in real conditions but also allow for a comparative evaluation against the modeled values. The final figure aggregates all the data to offer a global perspective on the agreement between experimental results and model predictions.

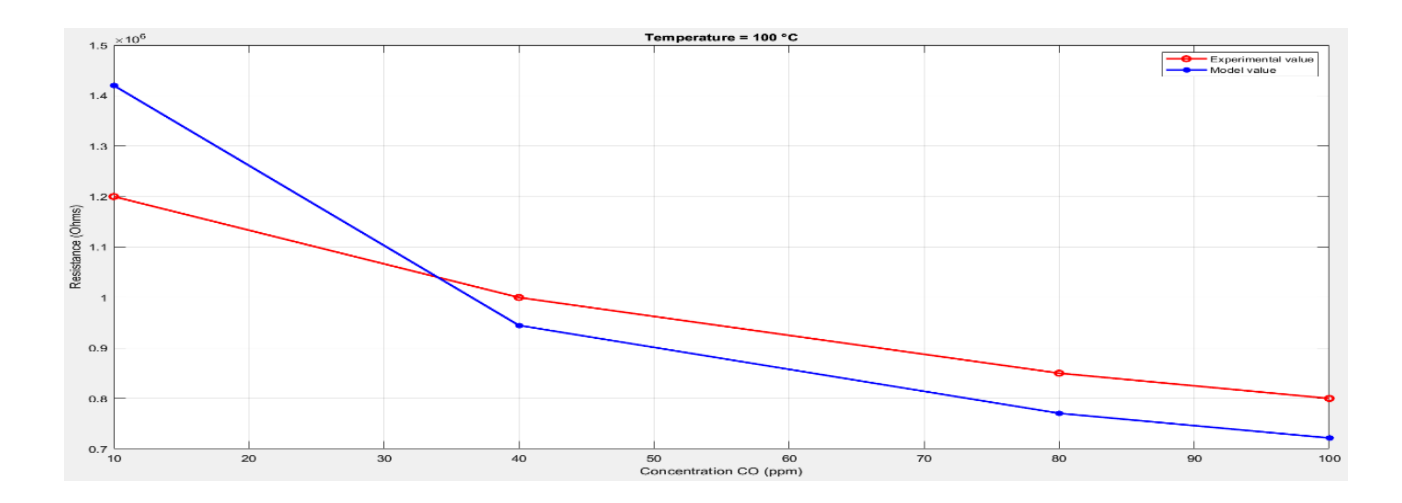


Figure III.12. Comparison of Experimental and Modeled Sensor Resistance at (T=100 Co)

• Temperature (100 °C):

This figure presents the experimental and modeled sensor resistance as a function of CO concentration at 100 °C. The experimental curve shows a gradual and consistent decrease in resistance as the concentration increases from 10 to 100 ppm. In contrast, the modeled curve starts at a significantly higher resistance and drops more sharply between 10 and 40 ppm before leveling off. There is a noticeable gap between the two curves, particularly at lower concentrations. This discrepancy indicates that the model overestimates the resistance at lower temperatures, possibly due to limitations in how it represents surface interactions or kinetic behavior.

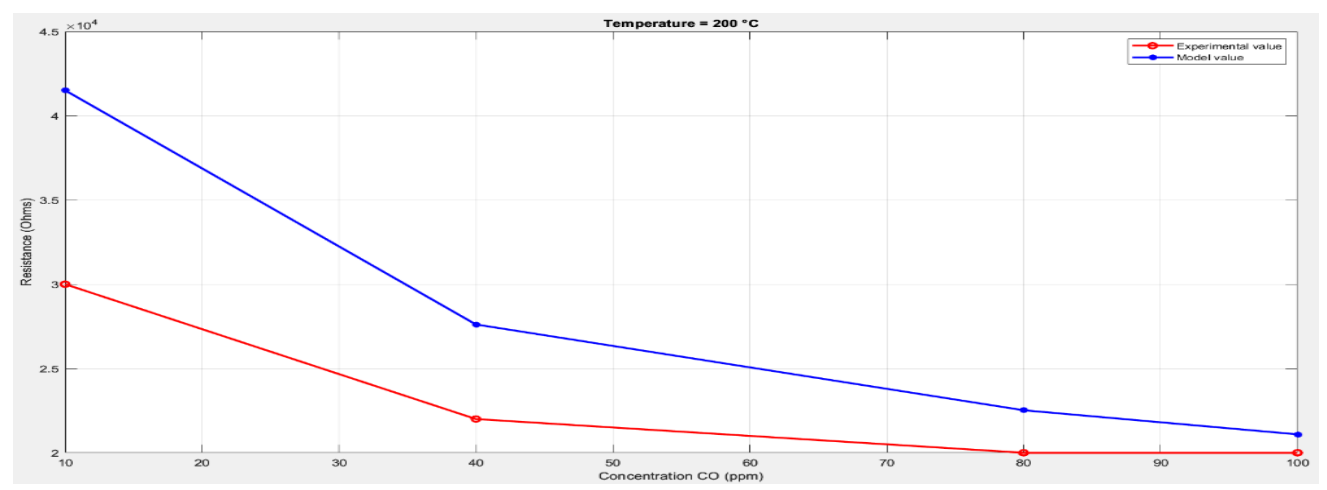


Figure III.13. Comparison of Experimental and Modeled Sensor Resistance at (T=200 Co)

• Temperature (200 °C)

At 200 °C, the experimental data continue to show a smooth decline in resistance with increasing CO concentration. The model follows a similar trend but still predicts higher resistance values across the range. Although the model approximates the experimental data more closely at 80 and 100 ppm, the mismatch persists throughout. This suggests that while the model becomes more accurate at this intermediate temperature, it still does not fully capture the sensor's actual response.

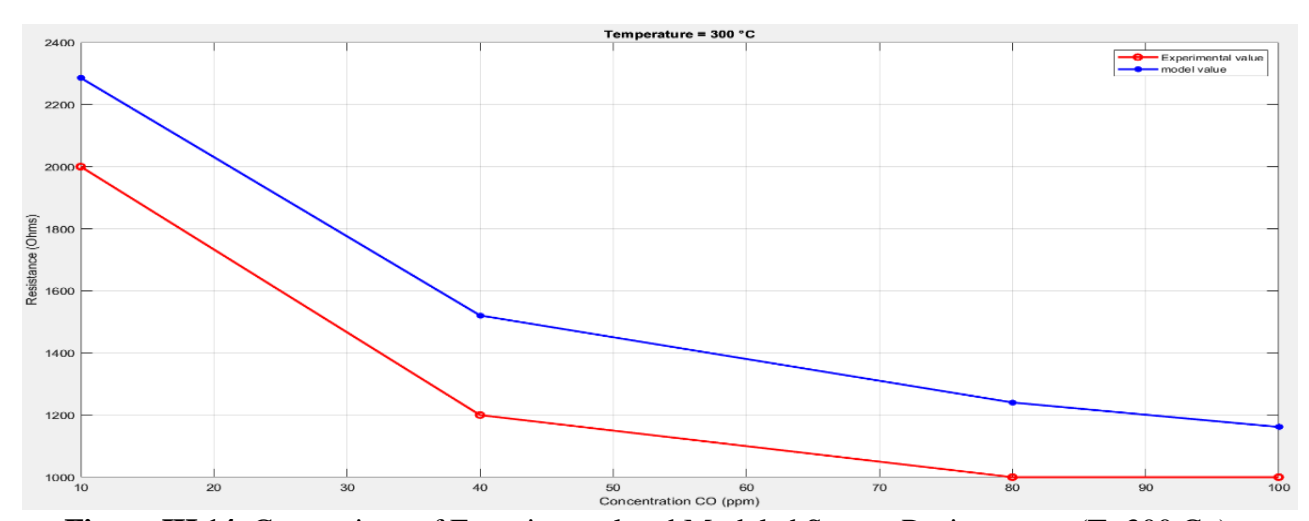


Figure III.14. Comparison of Experimental and Modeled Sensor Resistance at (T=300 Co)

• Temperature (300 °C):

In this figure, the experimental resistance decreases more sharply at low concentrations and begins to plateau after about 60 ppm. The modeled curve successfully mimics this general shape and behavior, and the overall alignment between model and experiment is improved compared to the lower temperatures. Despite a remaining difference in absolute resistance values, the model appears more reliable at this higher temperature

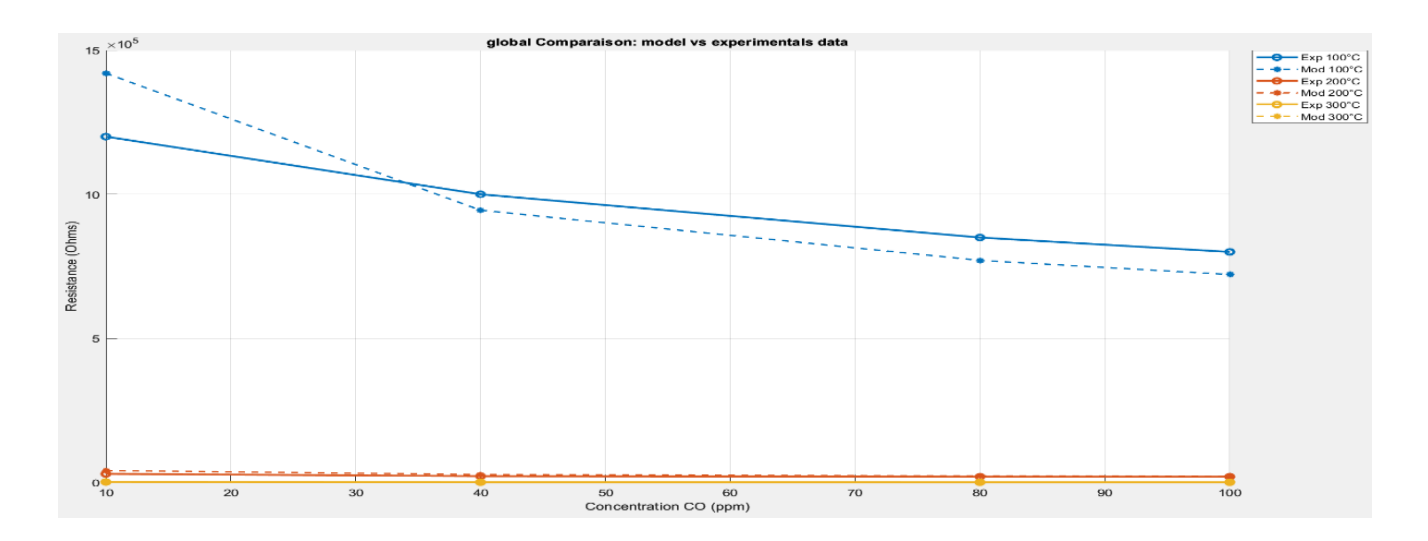


Figure III.15. Comparison of Experimental and Modeled Sensor Resistance at at Varying Temperatures

• Combined Comparison

This global figure overlays experimental and modeled curves for all three temperatures. It illustrates the model's performance across the temperature range. At 100 °C, the model significantly overpredicts resistance. At 200 °C and 300 °C, the model begins to match the experimental trend more closely, especially at higher concentrations. However, deviations remain, particularly at lower concentrations and lower temperatures. The model is qualitatively consistent with experimental observations but quantitatively less accurate, especially under cooler conditions.

III.5.1 Conclusion

The experimental results show a clear decrease in sensor resistance with increasing CO concentration at all three temperatures, which aligns with the expected behavior of a typical n-type metal oxide gas sensor. However, discrepancies between the model and experimental data are evident across all cases.

At 100 °C, the model slightly overestimates the resistance at lower concentrations but converges closer to the experimental data at higher CO levels. At 200 °C and 300 °C, the model continues to overestimate resistance values, particularly at lower concentrations, although it generally follows the same decreasing trend observed experimentally. These discrepancies suggest that while the model captures the general response pattern of the sensor, it lacks precise

accuracy, especially under dynamic real-world conditions.

The global comparison figure consolidates this observation, illustrating that while the modeled curves follow the overall behavior of the experimental data, the degree of deviation varies with temperature. The gap between modeled and actual values narrows slightly at higher concentrations, indicating that the model may be more reliable under conditions of elevated CO levels.

These results confirm the importance of integrating experimental validation into sensor development and model refinement. The deviations observed can be attributed to factors such as environmental conditions, surface states of the sensor material, or simplifications within the model itself. Overall, this comparison emphasizes the necessity of iterative calibration between theory and practice to improve predictive accuracy and sensor reliability.

General conclusion

General conclusion

Mathematical modeling of ZnO resistance as a function of CO concentration provides a simple but effective framework for understanding and exploiting the behavior of this material in gas sensors. The empirical approach based on the $R=R0(T)\cdot C^{-n(T)}$ law allows to integrate the effects of temperature via R0 and n. The results obtained clearly show the importance of controlling the heating temperature to optimize the sensitivity of the sensor. This study can be extended to other sensitive gases or materials, and serve as a basis for the simulation-assisted design of smart sensors.

Bibliographic references

Bibliographic references

- [1] Abbas, B. M. (2017). Impact of temperature on the sensitivity of ZnO to carbon monoxide. Doctoral thesis, University of Constantine.
- [2] Yamazoe, N. & Shimanoe, K. (2009). New perspectives of gas sensor technology. Sensors and Actuators B: Chemical, 138, 100–107.
- [3] Zimmer, P. (2007). Structure–property–function relationships in nanoscale oxide sensors: a case study based on zinc oxide. Advanced Functional Materials, 17, 1385–1391.
- [4] Wang et al. (2020). Multiphysics simulation of a ZnO-based sensor.
- [5] Baruah, S., & Dutta, J. (2009). Hydrothermal growth of ZnO nanostructures. Science and Technology of Advanced Materials, 10(1), 013001.
- [6] Draper, N. R., & Smith, H. (1998). Applied Regression Analysis. 3rd Edition. Wiley.
- [7] Radhakrishnan, J. K., & Geetika, M. K. (2021). Effect of temperature modulation on the gas sensing characteristics of ZnO nanostructures for O₂, CO, and CO₂ gases. Sensors International, 2, 100059.
- [8] González-Vidal, J. L., De la L. Olvera, M., Maldonado, A., Reyes-Barranca, A., & Meléndez-Lira, M. Sensibilité au CO de films minces de ZnO non dopé, Cr-ZnO et Cu-ZnO obtenus par pyrolyse en spray.